Physics-Informed Machine Learning for Ultrasonic Guided Wave Full-Field Reconstruction and Damage Diagnosis

ALBERTO CASARTELLI, LUCA LOMAZZI, LUCIO PINELLO, RAFAEL JUNGES, MARCO GIGLIO and FRANCESCO CADINI

ABSTRACT

Ultrasonic guided waves have shown significant efficacy in structural health monitoring due to their increased sensitivity to structural changes in mechanical properties. Particularly, they are advantageous for the detection, localization, and quantification of damage in thin-walled structures. Traditional diagnostic methods that utilize ultrasonic guided waves often depend on signal pre-processing to extract pertinent features, which may inadvertently lead to the loss of crucial information. Recent advancements have seen the incorporation of neural networks to circumvent pre-processing and allow for the direct analysis of complex signals. However, the blackbox nature of neural networks, their dependence on extensive labeled data sets, and limitations in generalizing beyond their training domain present considerable challenges. This study introduces a novel unsupervised physics-informed machine learning methodology aimed at overcoming these obstacles. The damage diagnosis problem is framed as an inverse problem, specifically a full-waveform inversion task, with the objective of reconstructing the material distribution throughout the structure to identify potential discontinuities caused by damage. The methodology combines neural networks with a custom finite difference solver capable of efficiently simulating wave propagation, embedding the physics of the problem into the solution. The proposed methodology was validated against a case study of a metal plate affected by a single damage. Despite the computational challenges posed by the three-dimensional nature of the problem, the findings indicate that the approach effectively localizes and quantifies damage within the investigated structure.

INTRODUCTION

Traditional Lamb Wave (LW)-based Structural Health Monitoring (SHM) methods employ tomographic algorithms [1] to reconstruct damage maps, requiring manual Damage Index (DI) extraction [2] and relying on empirical formulas or assumptions that

Alberto Casartelli, PhD Student, Email: alberto.casartelli@polimi.it. Luca Lomazzi, Research Fellow, Email: luca.lomazzi@polimi.it. Lucio Pinello, PhD Candidate, Email: lucio.pinello@polimi.it. Rafael Junges, PhD Candidate, Email: rafael.junges@polimi.it. Marco Giglio, Professor, Email: marco.giglio@polimi.it. Francesco Cadini, Associate Professor, Email: francesco.cadini@polimi.it. Department of Mechanical Engineering, Politecnico di Milano, Milan, MI, IT

limit non-linear damage characterization. Supervised Machine Learning (ML) techniques such as Neural Networks (NN) automate detection by capturing non-linear relationships but remain DI-dependent, offering partial improvements [3, 4]. Unsupervised ML approaches [5, 6] bypass DI extraction by analyzing raw LW signals directly, but are computationally intensive. Besides, Supervised and Unsupervised ML are domain-specific and suffer from "black-box" interpretability issues, critical for safety-focused SHM. Physics-Informed Machine Learning (PIML) integrates physical laws into ML, creating interpretable "gray-box" models [7]. However, LW-based PIML research remains in its early stages. This work proposes a novel PIML framework reformulating damage diagnosis as a Full Waveform Inversion (FWI) problem, combining a neural network for material property prediction with a physics-constrained Finite Difference Solver (FDS). Validated on an aluminum plate, the method successfully localizes and quantifies damage.

METHODOLOGY

The FWI-based damage diagnosis framework reconstructs material property distributions (identifying damage as discontinuities) using sparse LW measurements. The NN uses a Gaussian noise input to predict material properties at all spatial points. Predictions drive the FDS to simulate LW propagation using the governing Partial Differential Equations (PDEs). The loss is computed comparing the reconstructed signals (FDS outputs at sensor locations) to previous measurements from pitch-catch sensing using piezoelectric transducers (PZTs). The NN weights are updated through back-propagation using automatic differentiation until convergence (Figure 1). Measurements are numerically generated using the same FDS solver as in the inversion process to ensure simulation flexibility.

Analytical Equations and Finite Difference Solver

LW propagation is governed by PDEs combining elasticity and 3D Hooke's law, linking stress tensor components ($\sigma_{xx}, \sigma_{yy}, \sigma_{zz}, \sigma_{xy}, \sigma_{xz}, \sigma_{yz}$), displacements ($u_x, u_y, u_z$), and material properties. To model damage, the Young's modulus (E) was spatially pa-

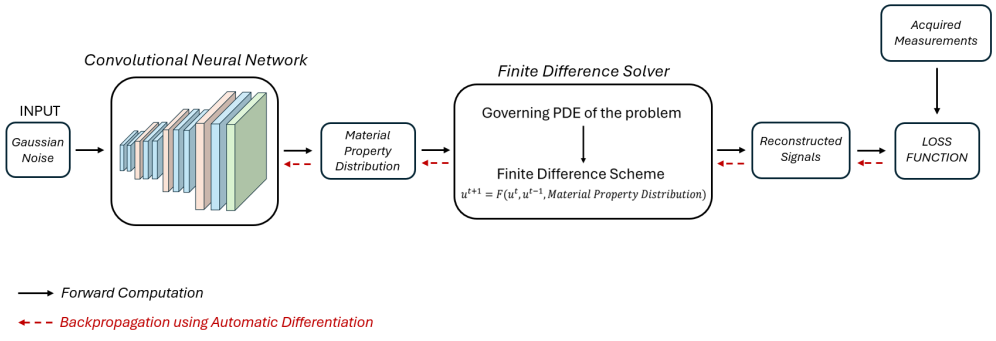

Figure 1. Damage Diagnosis FWI Framework

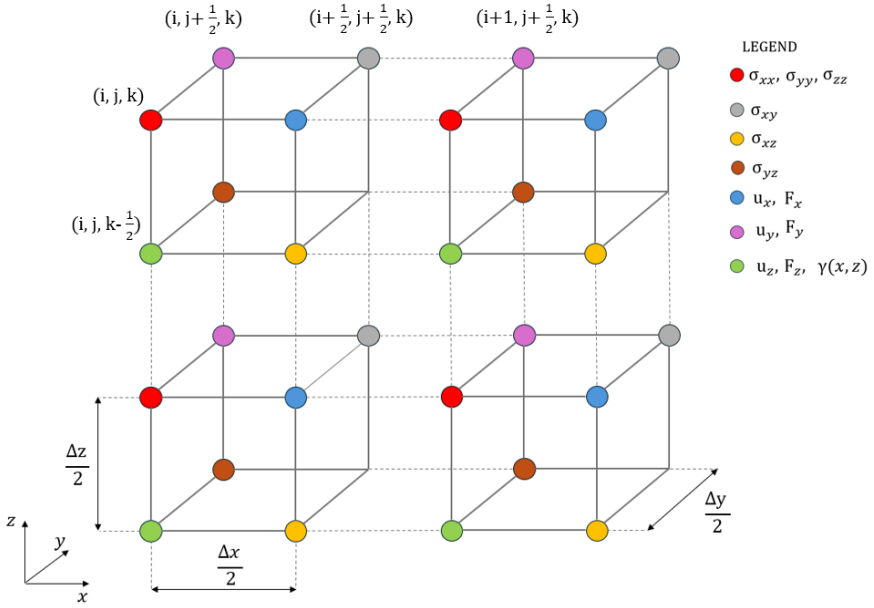

Figure 2. Layout of 3D staggered-grid, which is composed by repeated unit cells. Each wave-field variable and media parameter are defined at a specific node.

rameterized as:

$$E(x, y, z) = \gamma(x, y, z) \cdot E_0, \tag{1}$$

where $\gamma(x, y, z) \in [0, 1]$ quantifies stiffness reduction (damage), and E_0 represents the undamaged state.

An explicit, second-order, staggered-grid FDS, similar to [8], was developed to solve the LW propagation PDEs, introducing the physics-based component of the method (Figure 2). The 3D domain is discretized into a uniform grid ($\Delta x/2 = \Delta y/2 = \Delta z/2$). Stress and displacement variables are computed at staggered grid points. Each grid point is spatially indexed by (i, j, k). Simulation time L_t is discretized into time steps $\Delta t/2$, indexed by n.

The staggered-grid approach spatially and temporally decouples displacement and stress updates. The indicator function $\gamma(x, y, z)$ is defined at the green nodes, with intermediate values computed via arithmetic averaging. Free-surface boundary conditions (applied along z) and Dirichlet conditions (along x and y) are enforced using the stress-imaging technique [9], which sets σ_{xz} and σ_{yz} to zero at the free surfaces and imposes anti-symmetry for σ_{xx}, σ_{yy}, σ_{zz} and σ_{xy}. The external z–direction force was distributed as f_z/dV across 25 grid points to reduce numerical dispersion. Dirichlet boundaries and initial conditions are implemented via imaging and homogeneity, respectively. The solver was validated against Abaqus.

Neural Network Architecture

The proposed methodology employs a Convolutional Neural Network (CNN) to solve the FWI problem. It estimates the indicator function $\gamma(x, y, z)$, which parametrizes the Young's modulus of the structure. The CNN's structure is inspired by the common generator architecture of Generative Adversarial Networks (GANs). It takes Gaussian

TABLE I. ARCHITECTURE OF THE CNN.

Layer	**Shape After Layer**	**Learnable Parameters**
Input	$512 \times 25 \times 25 \times 6$	0
3D Conv + PReLU	$512 \times 25 \times 25 \times 6$	7,078,400 + 1
3D Conv + PReLU	$256 \times 25 \times 25 \times 6$	3,539,200 + 1
Upsample	$256 \times 50 \times 50 \times 6$	0
3D Conv + PReLU	$128 \times 50 \times 50 \times 6$	884,864 + 1
3D Conv + PReLU	$64 \times 50 \times 50 \times 6$	221,248 + 1
Upsample	$64 \times 100 \times 100 \times 6$	0
3D Conv + PReLU	$64 \times 100 \times 100 \times 6$	110,656 + 1
3D Conv + PReLU	$32 \times 100 \times 100 \times 6$	55,328 + 1
Upsample	$32 \times 200 \times 200 \times 6$	0
3D Conv + PReLU	$32 \times 200 \times 200 \times 6$	27,680 + 1
3D Conv + Sigmoid	$1 \times 200 \times 200 \times 6$	865 + 1
Total trainable parameters:		**11,918,249**

noise as input and returns $\gamma(x, y, z)$. The structure of these generator CNNs progressively expands, allowing the existing low-resolution layers to quickly converge, refining the representations by increasingly smaller-scale effects as new layers are introduced [10]. The result is an output tensor of higher resolution and a reduction of total training time.

Deviations from the indicator function ground-truth indicate damage. Training minimizes the Mean Square Error (MSE) between the FDS-reconstructed signals and measurements. The detailed architecture of the CNN is reported in Table I.

Adaptive activation functions are employed for convergence speed and output constraints: parametric ReLU (PReLU) accelerates training in hidden layers, while an adaptive Sigmoid ensures the final layer output remains in the range $[0, 1]$. Upsampling operations use nearest-neighbor interpolation, applied exclusively along the x and y directions given the low number of nodes along z. Training uses the Adam optimizer with a learning rate of 1×10^{-3} and gradient clipping with a threshold of 1×10^{-1} to stabilize convergence. Such values were identified as suitable empirically. The MSE between the FDS-reconstructed signals and ground-truth measurements drives the loss minimization.

A custom stop criterion was created to optimize training, based on the Root Mean Square Error (RMSE) between consecutive predictions of $\tilde{\gamma}(x, y, z)$. To smooth fluctuations in the RMSE, a moving average filter of 100 epochs was applied. Training terminates when the historical minimum of the filtered RMSE remains unchanged for 150 consecutive epochs, signaling convergence of the model.

This criterion ensures that the network has sufficiently stabilized and that further training will not yield significant improvements in the model's performance.

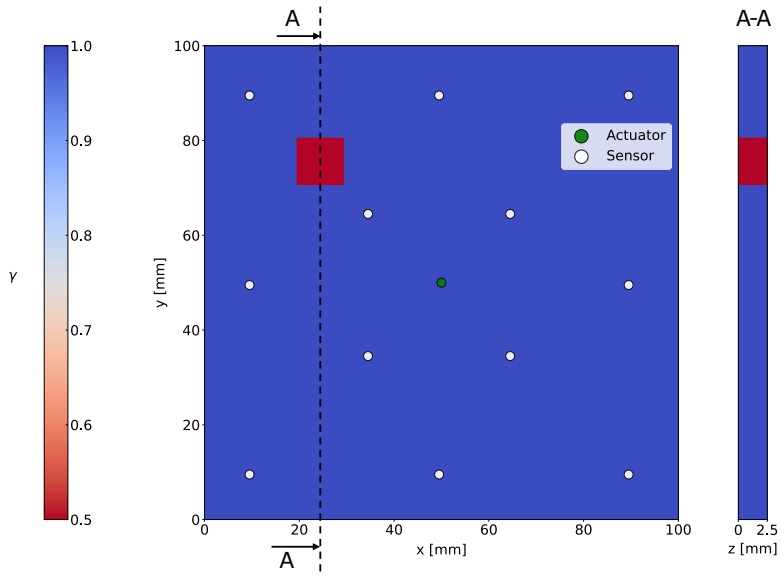

Figure 3. Orthogonal projection of the plate's upper surface indicator function distribution.

CASE STUDY

The case study consists of a 100 × 100 × 2.5 mm aluminum plate clamped on all four sides. The aluminum properties are as follows: $\rho = 2,700\ kg/m^3$, $\nu = 0.3$, $E_0 = 70$ GPa. Two forces with opposite phase are applied at the center of the plate on the opposite free-surfaces to excite the S_0 mode of LW propagation. The force time history is a Hanning-window-modulated sine wave, number of cycles $n_c = 3$ and excitation frequency $f = 200$ kHz. Twelve equally spaced sensors are placed on the upper surface to acquire the time history of u_z. The FDS uses a spatial discretization of $\Delta x = \Delta y = \Delta z = 0.5$ mm, resulting in a 201 x 201 x 6 grid. The time step is $\Delta t = 4 \cdot 10^{-8}$ s for a total simulation time of $L_t = 3.6 \cdot 10^{-5}$ s.

In the case study the presence of the damage is modeled as a single through-thickness discontinuity in the ground truth distribution of the indicator function $\gamma(x, y, z)$, which follows Equation 2.

$$\gamma(x,y,z) = \begin{cases} 0.5 & \text{for} \quad x \in [20,30] \quad \text{mm}, \quad y \in [70,80] \quad \text{mm}, \quad \forall z \\ 1 & \text{otherwise.} \end{cases} \tag{2}$$

Figure 3 shows an orthogonal projection of the plate, with the ground truth distribution of $\gamma(x, y, z)$ on the upper surface at the central view.

RESULTS AND DISCUSSION

The predicted $\tilde{\gamma}(x, y, z)$ and the corresponding residual absolute error are depicted in Figure 4. The central view shows the upper surface of the plate. The largest errors (approximately 30%) occur at the damage boundaries, due to the abrupt discontinuity

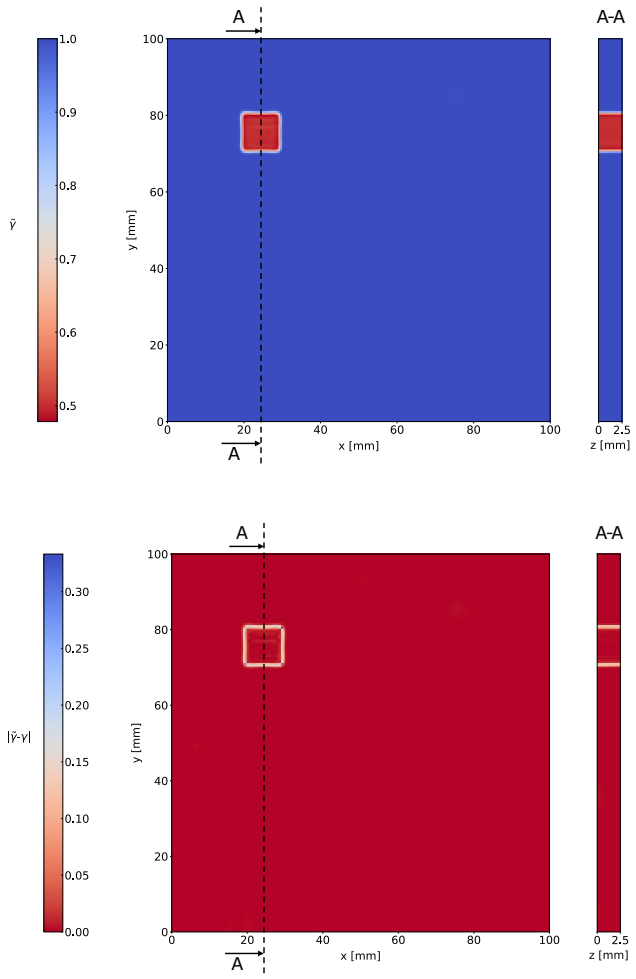

Figure 4. Indicator function distribution and the residuals for single-damage case study.

of the material property. However, these discrepancies are limited to narrow zones of approximately 1 mm (two nodes) at the boundaries of the damage region.

The Mean Relative Error (MRE_{dam}) in the prediction of $\tilde{\gamma}(x, y, z)$ within the damaged region is approximately 0.22%, suggesting that the error in the distribution of the predicted indicator function is nearly negligible. The training process lasted 618 epochs, for a total training time of 21.5 hours on an NVIDIA RTX 4060 GPU with 8 GB of VRAM.

CONCLUDING REMARKS

This study presents a PIML framework for damage diagnosis in thin-walled structures using LWs. The problem is framed as a FWI task to map the Young's modulus distribution. A NN predicts modulus variations, while an FDS simulates LW propagation via elastodynamic equations. The network parameters are optimized through automatic differentiation, minimizing the MSE between simulated and measured signals. A custom stop criterion (RMSE-based) reduces computational costs. Validated on

an aluminum plate with single through-thickness damage, the method achieved precise localization and quantification. Key conclusions are:

- The inversion approach is entirely unsupervised, requiring only signals acquired from the current state of the structure.
- The integration of the FDS ensures that the results are physically consistent.
- Raw LW signals are directly processed, avoiding any possible loss of information.
- The method is not domain-specific, provided that the FDS is able to model LW propagation through the given geometry.
- The high accuracy of the results comes at the cost of high computational effort.

In conclusion, while the method shows significant results in terms of damage diagnosis, its application to complex structures remains challenging. Future research involves extending the FWI-based approach to anisotropic composite structures and conducting experimental validation.

REFERENCES

1. Zhao, X., R. L. Royer, S. E. Owens, and J. L. Rose. 2011. "Ultrasonic Lamb wave tomography in structural health monitoring," *Smart materials and structures*, 20(10):105002.
2. Lomazzi, L., M. Giglio, and F. Cadini. 2023. "Towards a deep learning-based unified approach for structural damage detection, localisation and quantification," *Engineering Applications of Artificial Intelligence*, 121:106003.
3. Sbarufatti, C., G. Manson, and K. Worden. 2014. "A numerically-enhanced machine learning approach to damage diagnosis using a Lamb wave sensing network," *Journal of Sound and Vibration*, 333(19):4499–4525.
4. Nazarko, P. and L. Ziemianski. 2016. "Damage detection in aluminum and composite elements using neural networks for Lamb waves signal processing," *Engineering Failure Analysis*, 69:97–107.
5. Lomazzi, L., R. Junges, M. Giglio, and F. Cadini. 2024. "Unsupervised data-driven method for damage localization using guided waves," *Mechanical Systems and Signal Processing*, 208:111038.
6. Junges, R., Z. Rastin, L. Lomazzi, M. Giglio, and F. Cadini. 2024. "Convolutional autoencoders and CGANs for unsupervised structural damage localization," *Mechanical Systems and Signal Processing*, 220:111645.
7. Wua, Y., B. Sicarda, and S. A. Gadsdena. 2024. "A Review of Physics-Informed Machine Learning Methods with Applications to Condition Monitoring and Anomaly Detection," *arXiv:2401.11860*.
8. Graves, R. W. 1996. "Simulating seismic wave propagation in 3D elastic media using staggered-grid finite differences," *Bulletin of the Seismological Society of America*, 86(4):1091–1106.
9. Kristek, J., P. Moczo, and R. Archuleta. 2002. "Efficient Methods to Simulate Planar Free Surface in the 3D 4th-Order Staggered-Grid Finite-Difference Schemes," *Studia Geophysica et Geodaetica*, 46:355–381.
10. Karras, T., T. Aila, S. Laine, and J. Lehtinen. 2018, "Progressive Growing of GANs for Improved Quality, Stability, and Variation," .